Nanoscale

Ultrafast, Asymmetric Charge Transfer and Slow Charge Recombination in Porphyrin/CNT Composites Demonstrated by Time-Domain Atomistic Simulation

Journal:	*Nanoscale*
Manuscript ID	NR-ART-03-2018-002544.R1
Article Type:	Paper
Date Submitted by the Author:	19-May-2018
Complete List of Authors:	Sarkar, Ritabrata; University of Gour Banga Habib, Md.; University of Gour Banga, Chemistry Pal, Sougata; University of Gour Banga Prezhdo, Oleg; University of Southern California, Chemistry

Ultrafast, Asymmetric Charge Transfer and Slow Charge Recombination in Porphyrin/CNT Composites Demonstrated by Time-Domain Atomistic Simulation

Ritabrata Sarkar[†], *Md Habib*[†], *Sougata Pal*[†, ‡, *], *Oleg V. Prezhdo*[‡, *]

[†]*Department of Chemistry, University of Gour Banga, Malda, 732103, India*

[‡]*Department of Chemistry, University of Southern California, Los Angeles, CA 90089, USA*

ABSTRACT

The versatile photochemical properties of porphyrin molecules make them excellent candidates for solar energy applications. Carbon nanotubes (CNTs) exhibit superior charge conductivity and have been combined with porphyrins to achieve efficient and ultrafast charge separation. Experiments show that the charge separated state lives less than 10 ps, which is too short for applications. Using real-time time-dependent tight binding density functional theory (DFTB) combined with non-adiabatic molecular dynamics (NAMD), we model photo-induced charge separation and recombination in two porphyrin/CNT composites. Having achieved excellent agreement with experiment for the electron transfer from the porphyrins to the CNT, we demonstrate that hole transfer can be achieved upon CNT excitation, although in a less efficient way. By exciting the CNT one can extend light harvesting into lower energies of the solar spectrum and increase solar light conversion efficiency. We also show that the charge separated state can live over 1 ns. The two orders of magnitude difference from the experimental lifetime could arise due to presence of defects or metallic tubes in the samples. The charge separated state is long-lived because the non-adiabatic electron-phonon coupling is very small, less than 1 meV,

and the quantum coherence is short, 15-20 fs. The excited states in the isolated porphyrins and CNT live around 100 ps, in agreement with experiments as well. The porphyrin/CNT interaction occurs through the π-electron systems of the two species. The non-radiative relaxation is promoted by both high and low frequency phonons, with higher frequency phonons playing more important roles in electron than hole relaxation. Low frequency phonons contribute significantly to decay of the charge separated state, because they modulate relative positions of the porphyrins and the CNT. The time-domain atomistic simulations provide a detailed understanding of the charge separation and recombination mechanisms, and generate valuable guidelines for optimization of photovoltaic efficiency in modern nanoscale materials.

Keywords: Porphyrins, carbon nanotubes, ultrafast charge transfer, charge recombination, tight-binding density functional theory, non-adiabatic molecular dynamics

1. Introduction

In the last few years, inorganic-organic hybrid photovoltaic systems have received enormous attention as they can establish cost effective and robust alternatives to conventional solar cells.[1-6] In order to operate efficiently, these systems should exhibit ultrafast photo-induced charge separation, and the produced charges should live sufficiently long to allow their transport to external electrodes and photo-catalytic sites. Such a scenario is realized by designing interfaces with built-in internal electric fields favoring charge separation. Without an interface, only an external electric field can separate the carriers leading to poor light-to-electricity conversion.[7] Considering these key processes, diverse strategies have been developed to interface donors and acceptors into novel nanohybrid architectures.[8-11]

Carbon nanotubes (CNTs) have emerged as promising materials for solar cell applications[12, 13] due to their large surface area, high absorption cross-sections, excellent electron accepting properties, and outstanding carrier mobilities. CNTs exhibit an exceptional environmental stability and resistance to photo bleaching, which is one of the major drawbacks of organic systems designed for carbon-based optoelectronics.[14, 15] Poor solubility of CNTs in common media, including both aqueous or organic solvents, often makes it hard to process CNTs and manufacture the desired device.[16, 17] Non-covalent self-assembled hybrids, involving π-π stacking interactions of CNTs with organic molecules, have been developed to overcome some of the processing bottlenecks, while preserving the high-quality transport and optical properties of CNTs.[18-21] Non-covalent attachment of aromatic species, such as conjugated polymers,[22] pyrenes,[23] anthracenes,[24, 25] and porphyrins[23] to CNT surfaces has become an active area of research.

The primary chromophore in photosynthesis, porphyrins absorb strongly in the visible region. They are chemically stable and exhibit optoelectronic properties that can be tuned by

chemical means.[26] As a result, porphyrins are considered for a broad range of applications, including solar cells,[27, 28] photodetectors[29] and light-emitting diodes.[30-32] Porphyrin aggregates can take shape of nanotubes, exhibiting interesting charge transfer properties and dynamics.[33, 34] Non-covalent composites of porphyrins with CNTs are promising candidates for solar cell applications, due to significant electronic coupling between the π-systems of the two species.[35-37] It has been shown[12, 37, 38] that the binding affinity of porphyrins to CNTs increases sharply as the porphyrin π-electron system is extended, showing strong van der Waals interactions. CNT chirality also influences the π-π interaction, with special attention dedicated to chiral CNTs with the indices (7,5), (8,6), (7,6) and (6,5).[23] For example, porphyrin hybrids with the (7,6) CNT, which has a narrower band gap, show considerably better charge separation compared to porphyrin hybrids with the (6,5) CNT, which has a wider bandgap.[23] The differences arise due to the larger electron transfer (ET) driving force in the CNT with the smaller gap, as well as differences in the porphyrin/CNT π-π interactions. A sufficiently large ET driving force is required in order to achieve efficient charge separation, especially in systems involving organic and few-dimensional components that have high exciton binding energies.[39-43]

A variety of scenarios for excited state dynamics are possible in porphyrin/CNT hybrids, Figure 1. Photo-excitation of the porphyrin results in ET from the porphyrin excited state to the CNT conduction band (CB). On the contrary, photo-excitation of the CNT leads to hole transfer (HT) from the CNT valence band (VB) to the porphyrin. The two charge separation events, process ① in Figure 1, compete with charge recombination inside each material, process ②. Once the charge separation is achieved one of the two ways, the charge separated state can also undergo electron-hole (e-h) recombination, process ③ in Figure 1. A successful photovoltaic hybrid requires that charge separation is much faster than e-h recombination, and that the charge-separated state is long-lived.

Focusing on porphyrin derivatives with extended π-electron systems, Zhong *et al.* investigated how the strength of the π-π porphyrin/CNT interaction depends on the size, shape and oligomeric length of the π-conjugated porphyrins.[12] Among the isomeric porphyrins with differently extended π-systems, mono-fused, doubly-fused *anti-* and doubly-fused *syn*-porphyrins exhibited different binding selectivities. It was found that isomers with linear π-systems fit to CNTs better than bent isomers with identical π-systems. Transient absorption experiments[12] indicated ultrafast, sub-picosecond photo-induced ET from porphyrins to CNTs. At the same time, the majority of the photo-generated charges recombined rapidly, over the course of just a few picoseconds. The latter fact is surprising because excited state lifetimes in pristine porphyrins and CNTs extend to hundreds of picoseconds,[44-49]and because charges separated between different materials are expected to live longer than excitons localized within each subsystem. In order to realize the full potential of porphyrin/CNT hybrids in photovoltaic and related applications, it is critical to evaluate whether charge-separated states can be long-lived and to establish a detailed understanding of the mechanisms and factors that govern the complex electron-vibrational dynamics initiated by a photo-excitation in porphyrin/CNT composites. This goal can be achieved by time-domain atomistic simulations that mimic time-resolved laser experiments in the most direct way.

The present work reports time-domain atomistic modeling of the electron and hole transfer, and e-h recombination in the two porphyrin/CNT hybrids studied experimentally.[12]By providing a detailed understanding of the mechanisms of the excited state processes, the study demonstrates that ET from the porphyrins to the CNT requires several hundred femtoseconds, in good agreement with experiment. It demonstrates a picosecond HT following photo-excitation of the CNT. The timescale differences are rationalized in terms of driving force, density of acceptor states, donor-acceptor coupling, quantum coherence, and participation of particular vibrational

modes. The calculated e-h recombination in the isolated porphyrins and CNT takes about 100 ps, in agreement with experiment. The charge separated state lives a nanosecond, in strong disagreement with the experiment. The discrepancy is rationalized by possible presence of defects or metallic CNTs in the experimental samples. The reported theoretical predictions regarding the picosecond HT and nanosecond e-h recombination in the defect-free system provide valuable guidelines for design of efficient solar harvesting materials. In particular, light absorption by CNTs followed by HT allows one to extend the spectral range of the harvested solar light. Existence of long-lived charges separated across the porphyrin/CNT interfaces demonstrates that the composites can lead to highly efficient solar devices, if material synthesis and purification can be improved.

2. THEORETICAL METHODOLOGY

The photo-induced charge transfer (CT) and recombination dynamics at the porphyrin/CNT interface have been studied using the recently developed methodology combining nonadiabatic (NA) molecular dynamics (MD) with the self-consistent charge density functional tight-binding (SSC-DFTB) theory [50] The fewest switches surface hopping (FSSH)[51, 52] and decoherence induced surface hopping (DISH)[53] approaches to NAMD have been formulated[54, 55] in the Kohn−Sham representation of DFT and adapted to the classical path approximation,[56, 57] which provides great computational savings and is justified in condensed matter systems. The electronic degrees of freedom are treated quantum mechanically, where as the nuclear degrees of freedom are treated (semi) classically. The nuclear evolutions are guided by quantum forces exerted by the electronic subsystem, while the electronic subsystem evolves under the influence of the classical external field generated by the nuclear subsystem. The FSSH[51, 52] and DISH[53] approaches are implemented within the Python eXtension for Ab Initio

Dynamics (PYXAID) software package,[56, 57] which was later adapted to the SSC-DFTB theory.[50]The methodology mimics time-resolved experiments in a most direct way and has been applied successfully to a broad range of relatively large systems.[48, 58-67]

2.1 Nonadiabatic Molecular Dynamics by Surface Hopping

The NAMD simulation requires calculation of adiabatic electronic state energies, NA couplings, and forces acting on the nuclei. These are computed in the framework of the SCC-DFTB method.[68-74] The time-dependent wave function of a system can be represented in the basis of Kohn-Sham orbitals as

$$\left|\psi(\mathrm{r};\mathrm{R(t)})\right\rangle = \sum_{k=0}^{N} c_{k(t)} \left|\phi_k(r;R(t))\right\rangle \qquad (1)$$

Where $c_k(t)$ is the time-dependent expansion coefficient, and $|\phi_k(r;R(t))\rangle$ is the adiabatic wave function representing the electronic state k, which is parametrically dependent on the classical nuclear trajectory $R(t)$. N is the size of the electronic basis set used in temporal evolution. The nuclear degrees of freedom are treated classically. The nuclear trajectories, $R(t)$, are obtained by solving the classical Newton's equations of motion using quantum-mechanical forces. The CPA allows one to use the ground state force. Evolution of the coefficients $c_k(t)$along a given classical trajectory can be obtained by solving the time-dependent Schrödinger equation

$$i\hbar \frac{dc_k(\mathrm{t})}{dt} = \sum_{i=0}^{N} (\varepsilon_k \delta_{ki} - i\hbar d_{ki}) c_i(t) \qquad (2)$$

Here, ε_k denotes energy of the adiabatic state k, and d_{ki} is the NA coupling between states k and i defined as

$$d_{ki} = \left\langle \phi_k(r, R(t)) \middle| \frac{\partial \phi_i(r, R(t))}{\partial t} \right\rangle \tag{3}$$

The NA couplings arise because electronic wave functions depend parametrically on nuclear coordinates. It reflects inelastic electron-phonon scattering. The coupling can be calculated numerically using the overlap of orbitals *k* and *i* at sequential timesteps[75, 76]

$$\begin{aligned} d_{ki} &= -i\hbar \left\langle \phi_k(r, R(t)) \middle| \nabla_R \middle| \phi_i(r, R(t)) \right\rangle \frac{dR(t)}{dt} \\ &= -i\hbar \left\langle \phi_k(r, R(t)) \middle| \frac{\partial}{\partial t} \middle| \phi_i(r, R(t)) \right\rangle \\ &\approx -\frac{i\hbar}{2\Delta t} \Big(\left\langle \phi_k(r, R(t)) \middle| \phi_i(r, R(t+\Delta t)) \right\rangle \\ &\quad - \left\langle \phi_k(r, R(t+\Delta t)) \middle| \phi_i(r, R(t)) \right\rangle \Big) \end{aligned} \tag{4}$$

Where Δt is the time step used for integration of the classical Newton's equation of motion. The numerical solution of eq (4) yields the time-dependent amplitudes of the adiabatic states, $c_k(t)$. The resulting amplitudes are utilized to calculate the probabilities of hopping between the electronic states. The many-electron version of the above equations can be found in Ref.[56]

FSSH is an algorithm for modeling electron-vibrational dynamics of mixed quantum-classical systems, combining the deterministic time dependent Schrodinger equations and stochastic sampling of electronic transitions.[51, 52] This method prescribes a probability of hopping between adiabatic electronic states between states *j* and *k* within a time interval *dt* computed from the time-dependent coefficients, Eq. (2):

$$dP_{jk} = \frac{-2\,\mathrm{Re}(a_{jk}^{*} d_{jk} . \dot{R})}{a_{jj}} dt; \quad a_{jk} = c_j^{*} c_k \tag{5}$$

A hop from state *j* to *k* is allowed only when the state population flows from *j* to *k*. If the hopping probability is found to be negative, it is set to zero. A uniform random number between 0 and 1 is generated in each time step and compared to the generated hopping probability to determine whether the hop will happen. The energy exchange between the electronic and nuclear degrees of freedom during the hop is assumed to be instantaneous. The velocity rescaling and hop rejection rules in the original FSSH scheme[51, 52] are replaced in the FSSH–CPA[56] by scaling the hopping probability upward in energy with the Boltzmann factor, which guarantees the detailed balance and quantum-classical thermodynamic equilibrium at the long time limit. In the present case, the FSSH method is applied in the CT processes, since they occur within quasi-continuous manifolds of states.

Mixed quantum-classical simulations of slow transitions across large energy gaps require decoherence corrections.[57, 77] This situation applies to the charge recombination processes in the current systems. The charge recombination is modeled using DISH,[53] which incorporates loss of quantum coherence into the quantum-classical approximation, developing on the idea that decoherence provides the physical mechanism for surface hops.[78] Transitions between quantum states occur in DISH at decoherence events. The decoherence time is computed as the pure-dephasing time of the optical response theory,[79]as described in Supporting Information.

2.2 Simulation Details

The simulation cells for the systems under investigation include a unit cell of the (7,6) CNT and a porphyrin molecule, as shown in Figure 2.30 Å of vacuum are added in the x- and y-directions, in order to avoid spurious interactions between simulation cell replicas. The CNT is periodic in the z-direction with the optimized cell length of 48.25 Å and the optimized tube diameter is 8.96 Å. The total number of atoms in the simulation cell is 657.

All quantum-mechanical calculations including geometry optimization, electronic structure, and adiabatic MD are carried out with the SCC-DFTB method as implemented in the DFTB+ code.[70, 80] The SSC-DFTB parameter set (Slater-Koster files) used in the calculations has been tested extensively for a broad range of compounds and can be found elsewhere.[81, 82] The density of states (DOS) has been computed using a 1×1×256 Monkhorst-Pack *k*-point mesh. The Lennard-Jones dispersion correction was employed.[83]

After the structure has been fully optimized, the systems have been heated to 300 K using velocity rescaling. Then, 5 ps micro canonical trajectories have been generated using the Verlet algorithm[84] with the 1 fs time step and Hellman–Feynman forces. At each time step, the energy of the Kohn–Sham molecular orbitals and the NA coupling matrix elements have been calculated, and this time-dependent information has been used to perform the NAMD simulation using the FSSH[51, 52] and DISH[53] methods, as implemented within the PYXAID program.[56, 57]

3. RESULTS AND DISCUSSION

Photovoltaic and photo-catalytic applications require long-lived charge separated states that are generated upon absorption of sun-light. Because optical selection rules necessarily lead to photo-excited states in which electron and hole wave functions overlap, photo-excitation has to be followed by efficient charge separation. The generated charges eventually recombine. Below we focus first on the geometric and electronic structure of the porphyrin/CNT composites, and discuss the electron-phonon interactions that drive the photo-induced dynamics. Then we consider the charge separation and recombination processes.

3.1. Geometric Structure

The knowledge of the geometry of a system constitutes the first step for analysis of the photo-induced CT dynamics, because the relative positions of various system components determine the strength of the donor-acceptor coupling, and ultimately the CT rate and mechanism. Figure 2 shows the top and side views of the relaxed geometries of the porphyrin/CNT composites at 0 K. The Zn atom is located at the center of the porphyrin core, and the *anti*- and *syn*-porphyrin systems differ in the way the two double-fused pyrenyl radicals attach to the porphyrin core, as discussed in detail in the experimental work.[12]The pyrenyls of the *anti*-isomer form a 180 degree angle, Figure 2a. The angle between the pyrenyls of the *syn*-isomer is less than 180 degrees, Figure 2b. The *anti*-isomer can wrap around the CNT better than the *syn*-isomer. The porphyrin and the two pyrenyls form a single extended π-electron system. The two 3,5-di-tert-butylphenyl groups that are also attached to the porphyrin core deviate from the π-electron plane, while also wrapping around the CNT. The *anti*-porphyrin forms a slightly better fit to the shape of the (7,6) CNT, as evidenced by the shorter *anti*-porphyrin/CNT distance (2.669 Å) compared to *syn*-porphyrin/CNT (2.719 Å). Donor-acceptor separations of this scale are suitable for formation of charge separated states.[85]

Figures S1 and S2 of Supporting Information show snapshots of the geometries of the two composites obtained from the MD trajectories at room temperature. Similarly to the optimized geometries, Figure 2, the porphyrins are curved, indicating that the porphyrin π-electron system interacts strongly with that of the CNT even at room temperature. The distance between the porphyrins and the CNT increase by about 0.3 Å at room temperature relative to 0 K. The small 10% distance increase due to thermal effects further supports the strong interaction between the π-electron systems of the two components. The orientations of the pyrenil substituents to the porphyrins fluctuate notably, showing that their interaction with the CNT is rather weak. The analysis of the geometric structure at zero and finite temperatures demonstrates

that that π-stacking is the donor-acceptor interaction giving rise to the ultrafast charge separation and slow recombination.

3.2. Electronic Structure

The relative energies of the donor and acceptor levels, together with the localization of the corresponding wave functions, are the key elements of the system's electronic structure governing the photo-induced dynamics. A large energy gap between the initial and final electronic states for a particular transition usually leads to slow dynamics, as exemplified by the charge recombination. If the wave functions are delocalized between the donor and acceptor species, as in the ET case, then a photo-excitation can generate a charge separated state, and the subsequent dynamics are accelerated due to strong donor-acceptor and NA electron-phonon couplings, and long quantum coherence.

Figure 3a shows the projected density of states (PDOS) of the *anti*-porphyrin/CNT composite under investigation at 0 K. The *syn*-porphyrin/CNT PDOS is similar and shown in Figure S3.The data demonstrate formation of a type-II photovoltaic heterojunction, as illustrated explicitly by the insets. The porphyrins exhibit discrete energy levels, while the CNT DOS contains sharp van Hove singularities separated by regions of relatively low DOS. A coincidence of a porphyrin level with a CNT singularity can lead to resonance effects, for instance, a particularly strong donor-acceptor coupling. No such coincidences are observed for either system. Although the result can be sensitive to the choice of the electronic structure method, the energy gaps between the porphyrin levels and CNT singularities are relatively large near the CB and VB edges, and a fortuitous coincidence is unlikely. The fact that the van Hove singularities and the discrete molecular levels characteristic of each species are also present in the combined system indicates that there is no covalent chemical bonding between the two components.

By tuning the photon energy and polarization, one can photo-excite either the porphyrin, or the CNT, or both. Excitation of the porphyrin leads to ET that proceeds from the porphyrin lowest unoccupied molecular orbital (LUMO) to the CNT LUMO localized within the first van Hove singularity. The energy region between the two LUMOs contains CNT states, which should facilitate the ET. In contrast, there are no energy levels between the highest occupied molecular orbitals (HOMO) of the porphyrin and the CNT, and a hop across this gap leading to the HT that follows CNT photo-excitation should be slower than the ET.

In order to ensure efficient CT, the corresponding driving force should be sufficiently large to overcome the Coulomb attraction between electron and hole, quantified by the exciton binding energy. Although the current work does not consider explicitly the excitonic effects, which require the Bethe-Salpeter theory that is extremely computationally expensive,[86, 87] we can compare the known exciton binding energies with the band offsets between the two systems, characterizing the driving force. The VB offsets are 0.2 eV for *anti* and 0.13 eV for *syn*, whereas the CB offsets are 0.30 eV for both systems, Table 1, Figures 3 and S3.The exciton binding energies of semiconducting CNTs range from 0.2 to 0.4 eV,[88-90]depending on CNT size, chirality, and dielectric constant of the surrounding medium that screens the Coulomb interactions. The exciton binding energies for porphyrins are in the 0.15-0.3 eV range depending on the number of interacting porphyrins.[91-93] The ET is driven by the 0.3 eV offset between the CB edges, which is sufficient to separate the electron and hole in the excited porphyrin. In comparison, the VB edge offset is equal to or smaller than the CNT exciton binding energy, indicating that an additional energy may be required for efficient HT, arising for instance from higher energy CNT excitations and leading to transfer of “hot” holes. The CB and VB offsets between the two subsystems also characterize the energy transferred from the electronic

subsystem to phonons during the CT processes. Such energy losses to heat reduce photon-to-current conversion efficiencies.

The charge separation yield depends on the donor-acceptor coupling, the strength of which is directly reflected by the extent of mixing between the donor and acceptor orbitals. The key electron and hole orbitals that enter the CT dynamics of the *anti*-porphyrin composite are shown in Figure 3b. The corresponding orbitals for the *syn*-porphyrin system are similar and shown in Figure S3b.The energies of these states are indicated by the vertical arrows extending from parts b to parts a of the figures. All orbitals are localized within the corresponding species with the exception of the porphyrin LUMO, which mixes with the orbitals of the CNT. The mixing occurs because the CNT has a continuous energy spectrum and contains states that are isoenergetic with the porphyrin LUMO. The delocalization of this orbital indicates that photo-excitation of the porphyrin already results in a partially charge-separated state, and that the subsequent dynamics should be fast due to donor-acceptor energy resonance.

Overall, the CNT DOS is higher than the porphyrin DOS, because the CNT contains more atoms, even if one considers only the CNT interaction region immediately next to the porphyrin. The density of donor and acceptor states is an important factor that determines the rates and efficiencies of photo-induced charge separation. The density of acceptor states is higher for the ET than the HT in the porphyrin/CNT hybrid.

Comparing all aspects of the electronic structure relevant to the ET and HT processes, we conclude that they are more favorable for the ET. The driving force is larger, the density of acceptor states is higher, and the donor-accepter state mixing is more significant for the ET than the HT.

3.3. Electron-Phonon Interactions

Vibrational motions play several key roles in the photo-initiated dynamics in the porphyrin/CNT hybrids. They promote ET and HT, while at the same time dissipating the excess electronic energy lost during the transfer processes. They create the NA coupling that promotes the non-radiative e-h recombination. Phonons are also responsible for loss of coherence within the electronic subsystem.

Figure 4 presents Fourier transforms of the energy gaps between the donor and acceptor states for (a) electron (blue) and (b) hole (red) transfer for the *anti*-composite. Parts (c) and (d) present the same data for the *syn*-composite. Both high and low frequency modes couple to electrons and hole, ranging from the 1600 cm^{-1} carbon-carbon stretching vibrations down to the CNT radial breathing modes (RBM) around 200 cm^{-1} and in-plane skeletal modes of the porphyrins.[94, 95]Generally, the slow large-scale motions modulate donor-acceptor distance and affect localization of the electronic states, while the fast local modes generate stronger NA coupling, which is proportional to the phonon velocity, Eq. (4), and are more efficient in dissipating large amounts of electronic energy, since they contain more energy per vibrational quantum.

The higher frequency modes are more important for the ET than the HT. A similar effect was observed in the ab initio study of intra band charge-phonon relaxation dynamics in CNTs.[58]It was attributed to the fact that electron states are supported by higher energy orbitals that contain more nodes, and therefore, electrons couple to vibrational modes that also have more nodes. The stronger coupling of the higher frequency modes to the electrons than the holes contributes to making the ET faster than the HT.

3.4. Decoherencein the Electronic Subsystem

Coupling to phonons induces loss of coherence in the electronic subsystem. The phases of the electronic wave functions for the initial and final states of a quantum transition get randomized, and the transition is slowed down, as exemplified by the quantum Zeno effect in the limit of infinitely fast decoherence.[59] The decoherence times are estimated here as the pure-dephasing times of the optical response theory.[79]The computation protocol is presented in Supporting Information. The pure-dephasing times can be measured experimentally either directly through time-resolved experiments, such as the photon-echo measurements,[96] or as inverse of the homogenous linewidth.[97]Generally, decoherence should be slow during charge separation and fast during charge recombination. Such situation would be most beneficial for enhancing of photovoltaic and photocatalytic activity.

The calculated pure-dephasing times are reported in Table 1 for the charge separation and Table 2 for the charge recombination. The decoherence events take between 10 and 100 fs, with charge separation and recombination showing similar times. A closer analysis shows a group of faster decoherence events, taking 15-20 fs, and three slower cases, requiring 50-90 fs. The differences can be rationalized by localization of the two wave functions involved in the transition in each case. If the wave functions are localized on different parts of the porphyrin/CNT hybrids, Figures 3b and S3b, decoherence is fast. It is also fast if both initial and final states are localized on the porphyrin, Table 2, which is relatively small and undergoes substantial thermal fluctuations, Figures S1 and S2. If the wave functions are significantly delocalized, either along the CNT, or between the CNT and a porphyrin, decoherence is slow. In particular, the ET donor states are delocalized between the porphyrins and the CNT. As a result, coherence is maintained for a long time during the ET process, Table 1. In contrast, the HT donor and acceptor states are localized on different parts of the porphyrin/CNT composites and

have very little overlap, leading to fast decoherence. Therefore, quantum coherence favors fast ET and slow HT.

3.5. Charge Transfer Dynamics

The dynamics of the photo-induced CT processes are characterized in Figure 5. Parts (a) and (b) describe the ET and the HT, respectively, in the *anti*-composite, while parts (c) and (d) are for the *syn*-composite. The dynamics are not purely exponential and contain a notable Gaussian component at early times. Therefore, the data were fitted to the combined Gaussian plus exponential function: $y=A\exp(-t/\tau_{exp})+(1-A)\exp(-0.5[t/\tau_{gau}]^2)$, and the timescales reported in Table 1 were obtained as the weighted average: $\tau=A\tau_{exp}+(1-A)\tau_{gau}$. Short-time quantum dynamics is always Gaussian (or cosine), because at early times the initial state transfers population to one or few most strongly coupled states, and a two-state system dynamics is described by the cosine function, known as the Rabi oscillation. Exponential decay is achieved at later times, when quantum dynamics span multiple states. Because the HT occurs from the CNT HOMO into the porphyrin HOMO, i.e. it involves a single final state, we fit the HT data to Gaussian only, i.e. A=0 for the HT. The ET takes place from the porphyrin LUMO into multiple unoccupied orbitals of the CNT, and therefore, it becomes exponential.

The ET is notably faster than the HT for several reasons. First, the density of acceptor states is higher for the ET, Figure 2, since it occurs from the porphyrins into the CNT, compared to the density of acceptor states for the HT, which takes place from the CNT into the porphyrins. Second, the initial state for the ET is delocalized onto the electron acceptor, while the initial state for the HT is localized solely on the donor, Figures 3b and S3b. As a result, a fraction of the electron is already transferred during photo-excitation of the porphyrin, and the quantum coherence time is longer for the ET than the HT. Third, the driving force (band offset) is larger for the ET than the HT, Figures 3a and S3a. Finally, the electron couples more strongly to the

higher frequency modes than the hole, Figure 4, and therefore, one may expect a stronger NA coupling. This is the case for the *anti*-composite, but not *syn*, Table 1. The larger NA coupling for the HT in the *syn*-porphyrin case can be rationalized by the small band offset, since the NA coupling is inversely proportional to the energy gap.[56] The NA couplings explain the relative differences between the two porphyrins. The ET is faster in the *anti*-porphyrin, because the corresponding NA coupling is larger, and for the same reason the HT is faster in the *syn*-porphyrin.

The calculated ET times show good agreement with the reported experimental value of 260 fs.[12] The calculated times are longer due to the finite size of the CNT in the simulation cell. CNTs are much longer in the experiments, and their DOS is higher. Because the ET occurs from the porphyrins into the CNT, the higher density of final states should lead to faster dynamics. In contrast, the porphyrins are identical in the experiment and simulation. Therefore, one may expect better agreement with experiment for the HT, which occurs between the CNT and porphyrin HOMOs. Note that no experimental data are available in this case.

3.6. Electron-Hole Recombination

Non-radiative e-h recombination constitutes the main source of charge and energy losses in solar energy applications. We consider the e-h recombination that follows charge separation across the porphyrin/CNT interface, and compare the interfacial recombination with that in the isolated porphyrins and CNT. The time-evolution of the excited state populations are presented for the two composites and the three isolated systems in parts a and b of Figure 6, respectively. The linear plots correspond to the short-time expansion of the exponential decay: $y=\exp(-t/\tau)\approx 1-t/\tau$. The corresponding time constants are presented in Table 2. Remarkably, the e-h lifetimes are an order of magnitude longer in the porphyrin/CNT composites than in the isolated systems. This is because the electron and hole states are localized on different parts the composites and exhibit

minimal overlap, Figures 3b and S3b. As a result the NA coupling matrix elements, Table 2, are very small, less than 1 meV. In comparison, the electron and hole wave functions in the isolated porphyrins and CNT overlap significantly, and the resulting NA coupling is 3-6 times larger. It is known that porphyrins and semiconducting CNTs have long-lived excited states that luminesce,[44-49, 98, 99] and the calculated nonradiative e-h recombination times for the isolated systems agree with the experimental data.[44-47, 98, 99]The time-resolved measurements performed on the porphyrin/CNT composites studied here show 6 ps e-h recombination times,[12]which are markedly shorter than the calculated 1 ns times. Most likely, the discrepancy arises because the simulation considers perfect systems, while CNTs in the experimental samples can contain defects or an admixture of metallic CNTs. Charge conductivity is very high in CNTs, and photogenerated charges can rapidly reach recombination sites. The calculation results show that the charge separated states can live in the porphyrin/CNT composites much longer than measured in the experiments,[12] and therefore, the composites can give efficient solar energy devices.

The vibrational modes contributing to the nonradiative e-h recombination in the porphyrin/CNT composites and the isolated systems are characterized in Figure 7, which presents Fourier transforms of the phonon-induced fluctuations of the energy gaps between the ground and excited states. The high-frequency G-mode is the main source of nonradiative e-h recombination in the pure CNT,[48, 49]Figure 7c. High-frequency vibrations are particularly efficient at facilitating the electron-phonon energy exchange during the e-h recombination across significant energy gaps, because a single quantum of such modes can accept a large fraction of the electronic energy. Both high and low frequency modes participate in the e-h recombination involving porphyrins. Just as in the CNT, high-frequency C-C stretches are efficient in accommodating large amounts of the electronic energy. The low frequencies appear because the

porphyrin molecules are much less rigid than the CNT and exhibit large scale, slow thermal fluctuations, Figures S1 and S2. The low frequency modes are particularly important in the porphyrin/CNT composites, because the charges reside on the different subsystems, and slow motions involving displacements of porphyrin and CNT relative to each other couple strongly to the e-h recombination transition.

4. CONCLUSIONS

In summary, by applying our recently developed methodology combining NAMD with SCC-DFTB, we have investigated photo-induced CT and recombination dynamics at the porphyrin/CNT interfaces. Our calculations show that upon photo-excitation of the porphyrins, an electron is transferred from porphyrin into the CNT on a sub-picosecond timescale, in good agreement with the experimental findings. We also predict that photo-excitation of the CNT leads to HT, which occurs on a picosecond timescale. The ET is faster than the HT due to a higher acceptor state density, greater hybridization of the donor and acceptor states, larger driving force, longer quantum coherence, and participation of faster phonon modes. The driving force is sufficient to overcome exciton binding energy for the ET; however, for the HT the driving force is similar to the exciton binding energy, and the HT is significantly slowed down. At the same time, charge separation resulting from photo-excitation of the CNT is advantageous because it requires lower energy photons and allows one to harvest a broader spectrum of sun-light. The porphyrins and the CNT couple through the π-electron system, with the porphyrins bending slightly to adjust to the CNT curvature. Compared to the CNT, the porphyrins undergo stronger thermal fluctuations, their pyrenil substituents in particular. The ET is faster for the *anti*-porphyrin/CNT composite, while the HT is faster for the *syn*-composite, as rationalized by the magnitudes of the NA coupling that depends on the donor-acceptor interaction and electronic

energy gap. The ET is faster in the *anti*-composite due to the better geometry match and stronger π-π stacking interaction. The HT is faster in the *syn*-composite due to the smaller energy gap.

The calculated e-h recombination times for the isolated porphyrins and CNT are on the order of 100 ps, in good agreement with experiments. Recombination of the charge separated state in the porphyrin/CNT composites takes an order of magnitude longer, around 1 ns. This finding contradicts strongly the experimental 6 ps time. The calculated e-h recombination in the porphyrin/CNT composites is long because the overlap between the electron and hole wave functions is small, and as a result, the NA is very small, less than 1 meV, and quantum coherence is short, 15-20 fs. The disagreement with the experiments can be rationalized by presence of CNT defects or metallic CNTs in the samples. Porphyrin/CNT composites based on defect-free semiconducting CNTs should support fast and long-lived charge separation, forming the basis for efficient solar energy applications. The non-radiative e-h recombination in the CNT is promoted by the high-frequency G-mode. Local high frequency vibrations and large scale low frequency motions contribute about equally to non-radiative relaxation in the porphyrins. Low frequency vibrations are particularly important for the non-radiative e-h recombination across the porphyrin/CNT interface, because they change relative positions of the porphyrins and the CNT, and most strongly affect the e-h overlap that governs the NA coupling. The reported simulations generate a comprehensive time-domain atomistic description of the charge separation and recombination dynamics in the porphyrin/CNT hybrids, provide valuable analysis of the experimental data, and suggest means of improving and maintaining charge separation needed for solar energy applications.

Author Information

*Corresponding Authors, E-mail: sougata@ugb.ac.in, prezhdo@usc.edu

Acknowledgements

R. S and S. P. acknowledge financial support from SERB-DST, Government of India through project Ref. No. CS-085/2014. O.V.P. acknowledges financial support from the U.S. Department of Energy, grant DE-SC0014429.

Supporting Information Available: Structural evolution of the two systems at room temperature, projected density of states and charge densities in the *syn*-porphyrin/CNT system, and calculation of the pure-dephasing times. The material is available free of charge via the Internet at http://pubs.acs.org.

Table 1. Canonically averaged band offset, absolute value of NA electron-phonon coupling, and decoherence and transfer times for electron transfer (ET) and hole transfer (HT) in the two porphyrin/CNT systems.

System	Process	Band offset (eV)	NA coupling (meV)	Decoherence (fs)	Transfer (fs)
anti-porphyrin/CNT	ET	0.30	5.81	52	473
	HT	0.20	2.06	16	2875
syn-porphyrin/CNT	ET	0.30	4.16	57	718
	HT	0.13	11.77	22	1010

Table 2. Canonically averaged absolute value of NA electron-phonon coupling, decoherence time and recombination time for electron-hole recombination across the porphyrin/CNT interfaces, in pristine CNT and in the porphyrins.

System	NA coupling(meV)	Decoherence(fs)	Recombination(ps)
anti-porphyrin/CNT	0.384	16	1070
syn-porphyrin/CNT	0.413	21	1060
CNT	1.352	89	146
anti-porphyrin	2.686	14	102
syn-porphyrin	2.910	14	88

FIGURE CAPTIONS

Figure 1. Diagram of energy levels involved in the photo-induced charge separation and recombination dynamics across the porphyrin/CNT interface. Photo-excitation of either porphyrin or CNT leads to charge separation①due to electron or hole transfer, respectively. Competing with the charge separation, electron and hole can undergo recombination② within the individual materials. Following charge separation the carriers can recombine at the interface③..

Figure 2. Optimized geometry of the porphyrin/CNT interface: **(a)** and **(b)** are top views of the *anti* and *syn* composites, whereas **(c)** and **(d)** show corresponding side views. The composites are held together by van der Waals and π-π interactions. The light and dark grey spheres denote C atoms in CNT and porphyrin, respectively. Light blue, purple and green spheres denote H, N, and Zn atoms, respectively.

Figure 3.(a) Projected density of states (PDOS) of the *anti*-porphyrin/CNT system at 0 K. The corresponding data for the *syn* composite is shown in Figure S3 of Supporting Information. The CNT has a much larger DOS than the porphyrin. Van Hove singularities of the CNT and discrete energy levels of the porphyrin are maintained in the combined system, indicating that the porphyrin/CNT interaction is non-covalent. The inset shows the energy offsets that drive electron and hole transfer. **(b)**Charge densities of the donor and acceptor states for the hole and electron transfer. The vertical arrows between panels (a) and (b) relate the donor and acceptor orbital densities to the orbital energies. The electron donor state is significantly delocalized between porphyrin and CNT, while the hole donor state is strongly localized on CNT. Both acceptor states are localized on the corresponding systems.

Figure 4. Fourier transforms of the energy gaps between the donor and acceptor states for the **(a)** electron transfer (blue) and **(b)** hole transfer (red) in the *anti*-porphyrin/CNT composite. Parts **(c)** and **(d)** show the same properties for the *syn*-porphyrin/CNT composite. The electron couples to both high-frequency C−C stretches and low frequency modes, where as the hole couples almost exclusively to the low-frequency modes. The strong involvements of high frequency modes accelerates electron transfer relative to hole transfer, Figure 5.

Figure 5. Photo-initiated electron and hole transfer dynamics across the porphyrin/CNT interface. Parts **(a)** and **(b)** represent population decay of electron and hole donor states for the *anti* composite, respectively, whereas **(c)** and **(d)**are the same for *syn*. The data are fitted with a linear combination of Gaussian and exponential functions. Electron transfer is faster than hole transfer due to the higher density of acceptor states, Figure 3, and involvement of high-frequency modes, Figure 4.

Figure 6. Charge recombination dynamics **(a)** across the *anti*-porphyrin/CNT (red line) and *syn*-porphyrin/CNT (blue line) interfaces, and **(b)** in pristine CNT (black), *anti*-porphyrin (magenta) and *syn*-porphyrin (indigo). The interfacial electron-hole recombination is an order of magnitude slower than recombination inside each material.

Figure 7. Fourier transforms of the energy gaps involved in the electron-hole recombination in **(a)***anti*-porphyrin/CNT, **(b)**syn-porphyrin/CNT, **(c)**pristine CNT, **(d)***anti*-porphyrin, and **(e)***syn*-porphyrin. Low frequency modes dominate non-radiative electron-hole recombination in the composite systems (a, b). Recombination in pristine CNT is driven by the high frequency G-mode (c). Recombination in the porphyrins is driven by both low and high frequency modes (d, e).

Figure 1

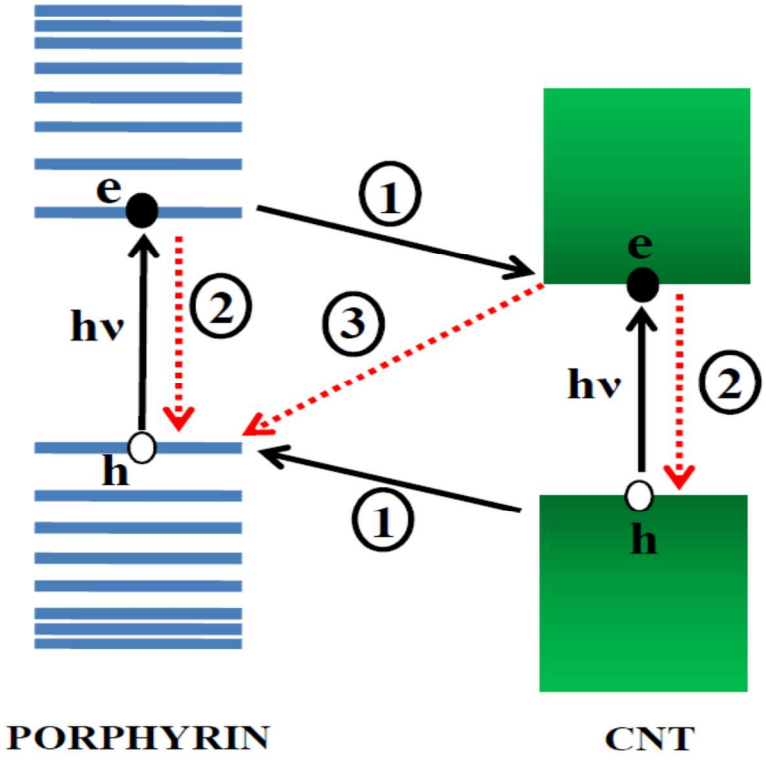

Figure 2

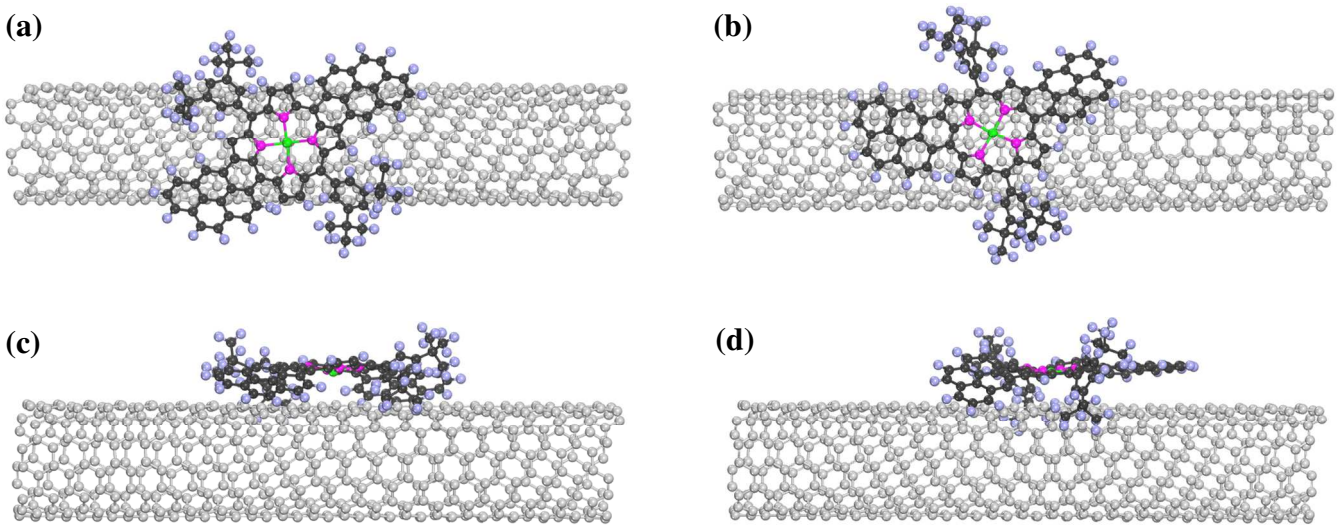

Figure 3

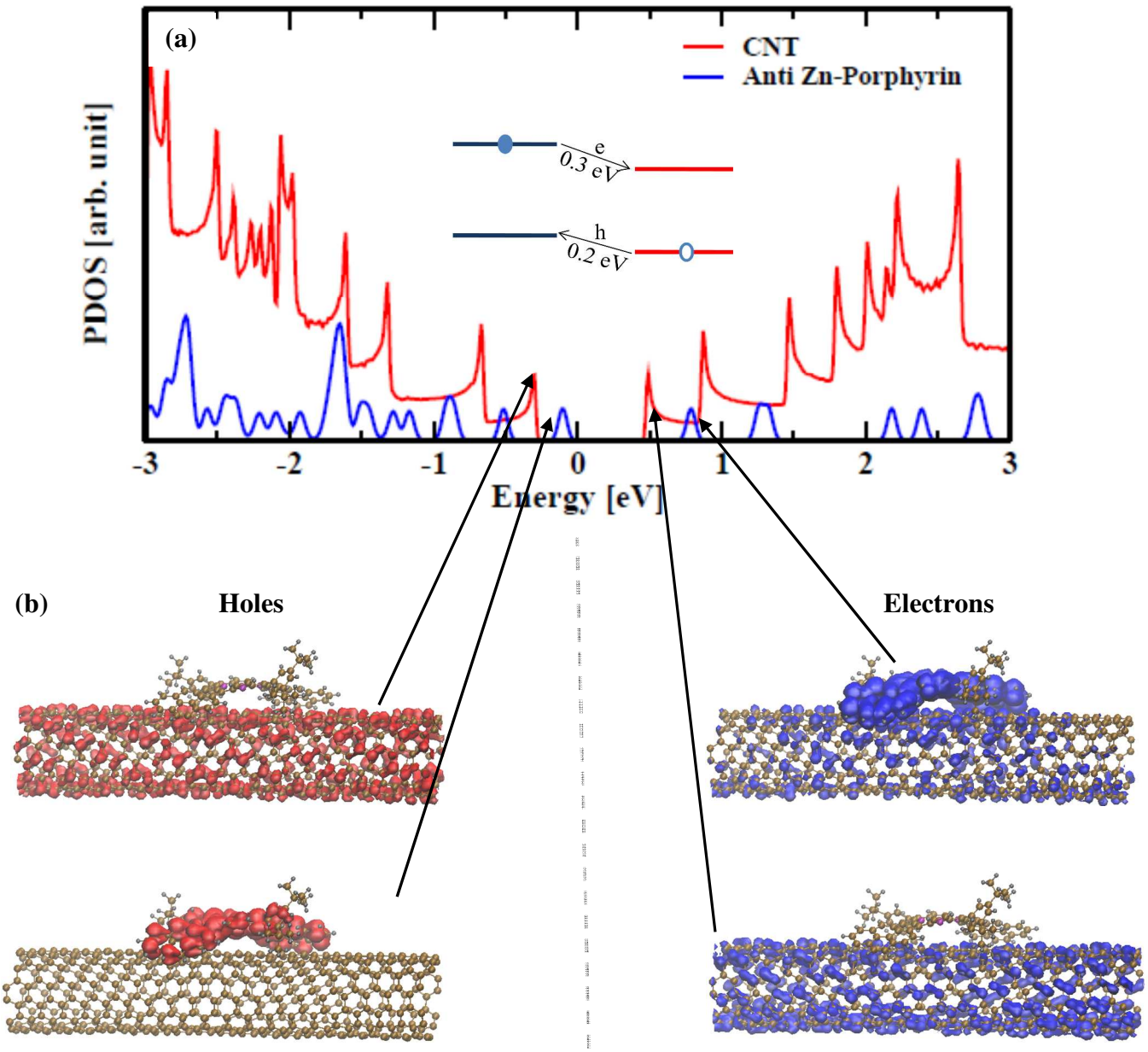
(a)
CNT
Anti Zn-Porphyrin
e
0.3 eV
h
0.2 eV
PDOS [arb. unit]
-3
-2
-1
0
1
2
3
Energy [eV]
(b)
Holes
Electrons

Figure 4

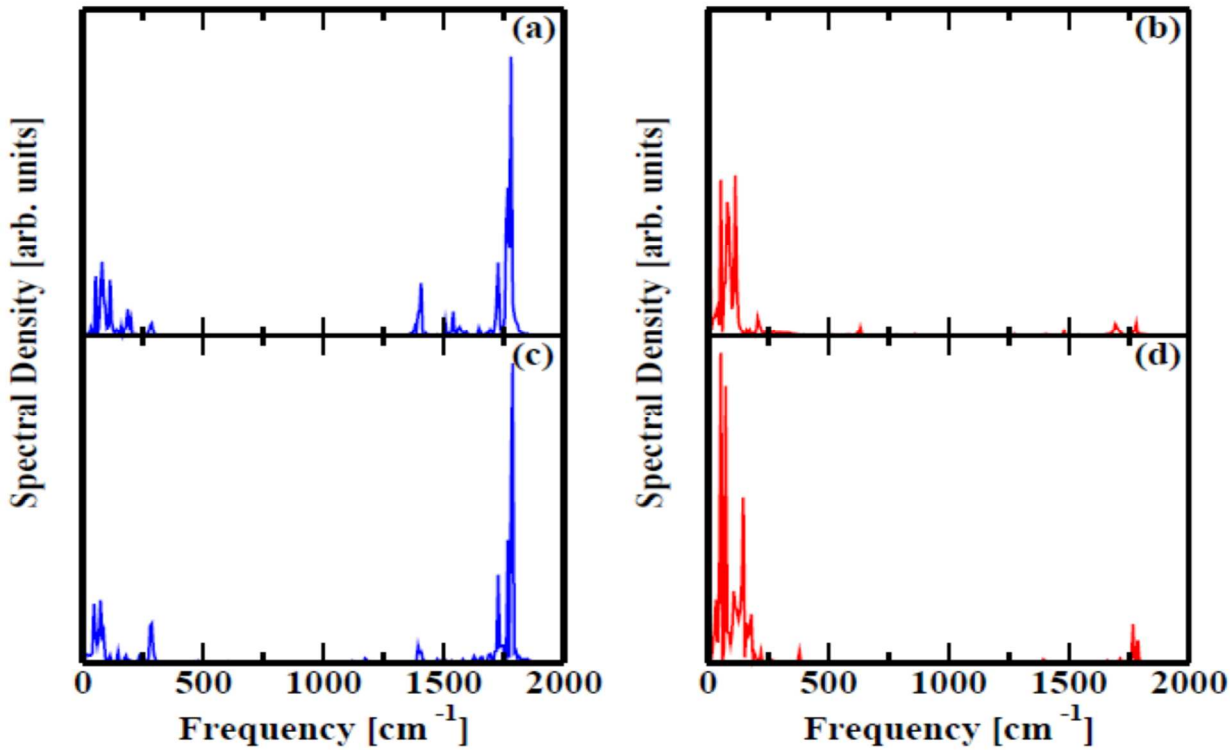
(a)
(b)
(c)
(d)
Spectral Density [arb. units]
Spectral Density [arb. units]
0
500
1000
1500
2000
Frequency [cm -1]
0
500
1000
1500
2000
Frequency [cm -1]

Figure 5

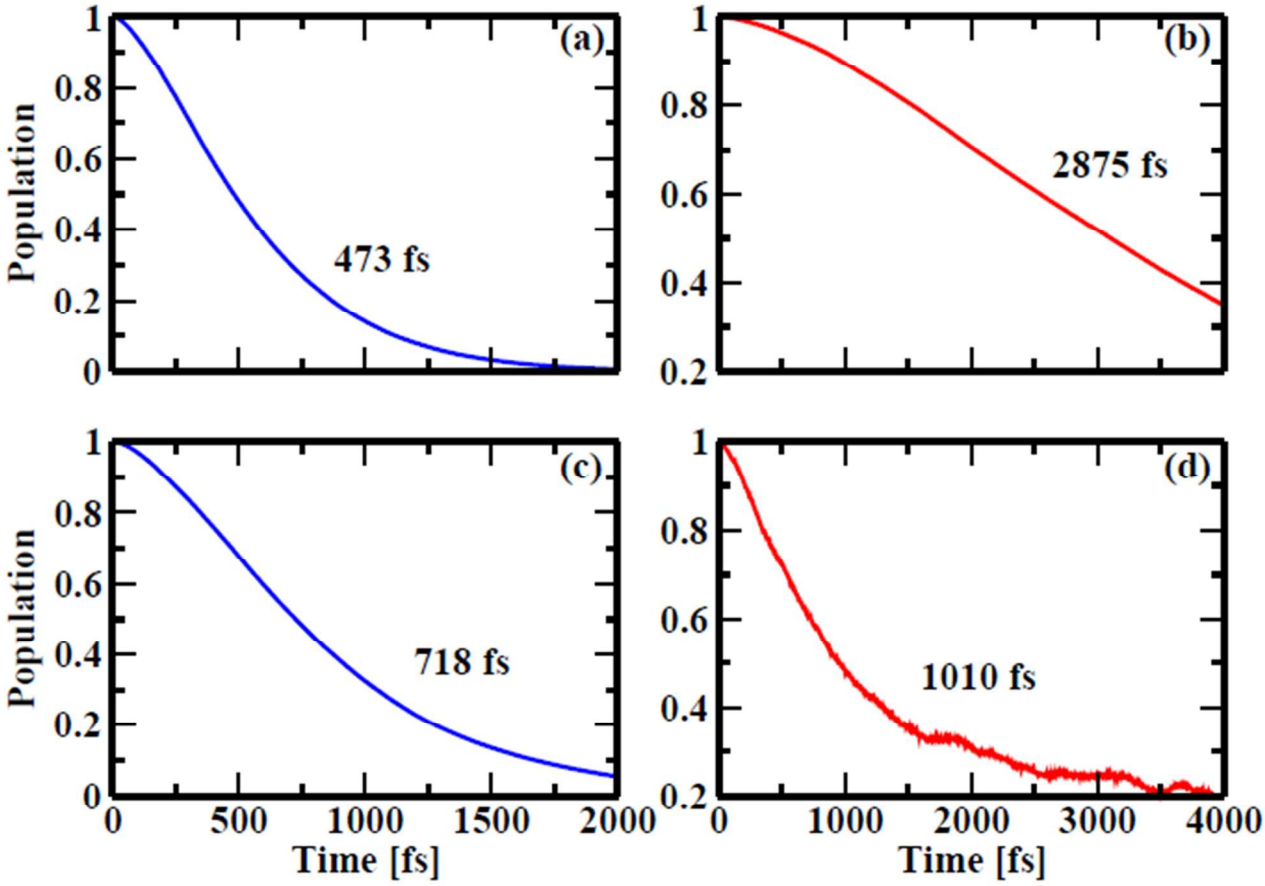
(a)
473 fs
(b)
2875 fs
(c)
718 fs
(d)
1010 fs
Population
Population
Time [fs]
Time [fs]
0
0.2
0.4
0.6
0.8
1
0
500
1000
1500
2000
0
1000
2000
3000
4000

Figure 6

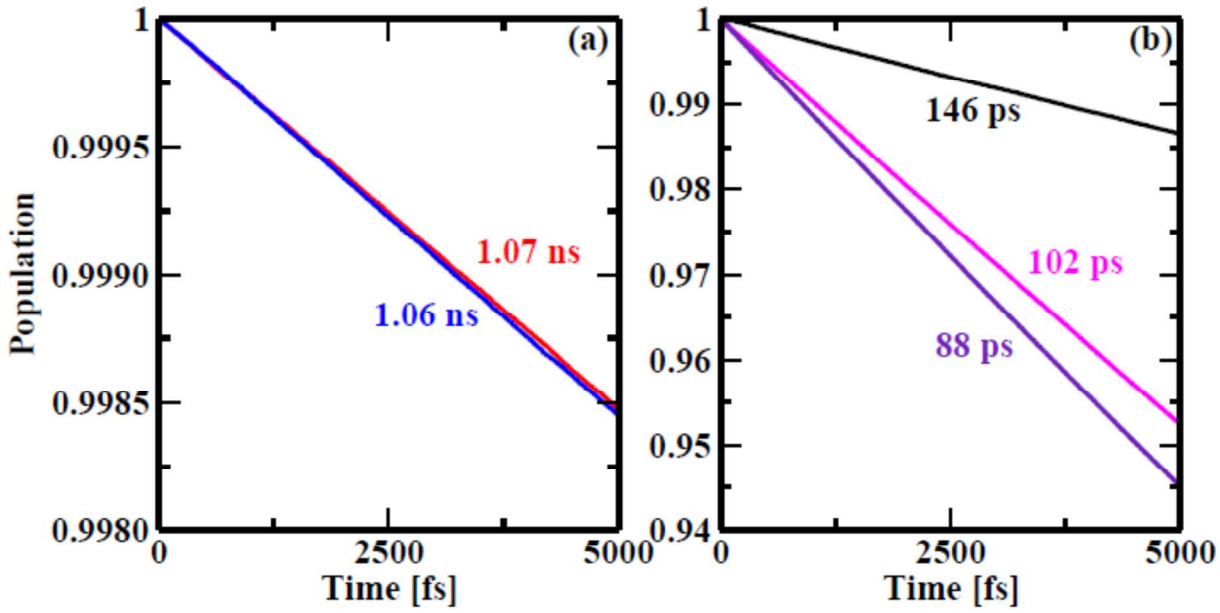
(a)
1
0.9995
0.9990
0.9985
0.9980
Population
1.07 ns
1.06 ns
0
2500
5000
Time [fs]
(b)
1
0.99
0.98
0.97
0.96
0.95
0.94
146 ps
102 ps
88 ps
0
2500
5000
Time [fs]

Figure 7

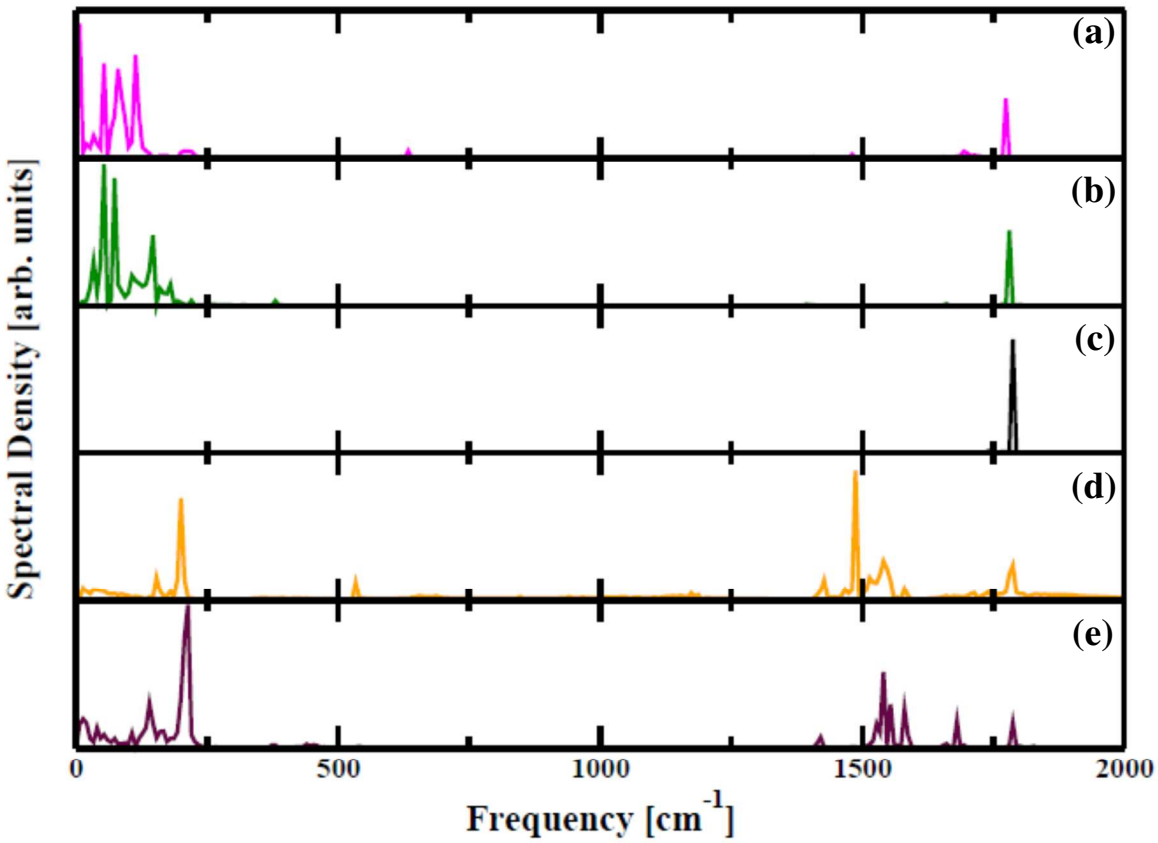
(a)
(b)
(c)
(d)
(e)
Spectral Density [arb. units]
0
500
1000
1500
2000
Frequency [cm-1]

References:

1. C. Draxl, D. Nabok and K. Hannewald, *Acc. Chem. Res.*, 2014, **47**, 3225-3232.

2. J. H. Heo, S. H. Im, J. H. Noh, T. N. Mandal, C.-S. Lim, J. A. Chang, Y. H. Lee, H.-j. Kim, A. Sarkar and M. K. Nazeeruddin, *Nat. Photonics*, 2013, **7**, 486-491.

3. S. Ren, L.-Y. Chang, S.-K. Lim, J. Zhao, M. Smith, N. Zhao, V. Bulović, M. Bawendi and S. Gradečak, *Nano Lett.*, 2011, **11**, 3998-4002.

4. S. Thiyagu, C.-C. Hsueh, C.-T. Liu, H.-J. Syu, T.-C. Lin and C.-F. Lin, *Nanoscale*, 2014, **6**, 3361-3366.

5. K. Sato, M. Dutta and N. Fukata, *Nanoscale*, 2014, **6**, 6092-6101.

6. J. Jung, Y. J. Yoon and Z. Lin, *Nanoscale*, 2016, **8**, 8887-8898.

7. B. Park, K. Whitham, J. Cho and E. Reichmanis, *ACS Nano*, 2012, **6**, 9466-9474.

8. A. E. Jailaubekov, A. P. Willard, J. R. Tritsch, W.-L. Chan, N. Sai, R. Gearba, L. G. Kaake, K. J. Williams, K. Leung and P. J. Rossky, *Nat. Mater.*, 2013, **12**, 66-73.

9. S. M. Lindner, S. Hüttner, A. Chiche, M. Thelakkat and G. Krausch, *Angew. Chem. Int. Ed.*, 2006, **45**, 3364-3368.

10. T. Stübinger and W. Brütting, *J. Appl. Phys.*, 2001, **90**, 3632-3641.

11. R. Nieman, H. Tsai, W. Nie, A. J. Aquino, A. D. Mohite, S. Tretiak, H. Li and H. Lischka, *Nanoscale*, 2018, **10**, 451-459.

12. Q. Zhong, V. V. Diev, S. T. Roberts, P. D. Antunez, R. L. Brutchey, S. E. Bradforth and M. E. Thompson, *ACS Nano*, 2013, **7**, 3466-3475.

13. Z. Li, P. P. Boix, G. Xing, K. Fu, S. A. Kulkarni, S. K. Batabyal, W. Xu, A. Cao, T. C. Sum and N. Mathews, *Nanoscale*, 2016, **8**, 6352-6360.

14. D. A. Heller, S. Baik, T. E. Eurell and M. S. Strano, *Adv. Mater.*, 2005, **17**, 2793-2799.

15. S. T. Huxtable, D. G. Cahill, S. Shenogin, L. Xue, R. Ozisik, P. Barone, M. Usrey, M. S. Strano, G. Siddons and M. Shim, *Nat. Mater.*, 2003, **2**, 731-734.

16. S. D. Bergin, V. Nicolosi, P. V. Streich, S. Giordani, Z. Sun, A. H. Windle, P. Ryan, N. P. P. Niraj, Z. T. T. Wang and L. Carpenter, *Adv. Mater.*, 2008, **20**, 1876-1881.

17. J.-Y. Hwang, U. S. Shin, W.-C. Jang, J. K. Hyun, I. B. Wall and H.-W. Kim, *Nanoscale*, 2013, **5**, 487-497.

18. P. Avouris, Z. Chen and V. Perebeinos, *Nat. Nanotechnol.*, 2007, **2**, 605-615.

19. A. S. Sandanayaka, R. Chitta, N. K. Subbaiyan, L. D'Souza, O. Ito and F. D'Souza, *J. Phys. Chem. C*, 2009, **113**, 13425-13432.

20. T. J. Simmons, J. Bult, D. P. Hashim, R. J. Linhardt and P. M. Ajayan, *ACS Nano*, 2009, **3**, 865-870.

21. J. Zhu, W. Cao, M. Yue, Y. Hou, J. Han and M. Yang, *ACS Nano*, 2015, **9**, 2489-2501.

22. A. Satake, Y. Miyajima and Y. Kobuke, *Chem. Mater.*, 2005, **17**, 716-724.

23. E. Maligaspe, A. S. Sandanayaka, T. Hasobe, O. Ito and F. D'Souza, *J. Am. Chem. Soc.*, 2010, **132**, 8158-8164.

24. F. Giroud and S. D. Minteer, *Electrochem. Commun.*, 2013, **34**, 157-160.

25. J. P. McNamara, R. Sharma, M. A. Vincent, I. H. Hillier and C. A. Morgado, *Phys. Chem. Chem. Phys.*, 2008, **10**, 128-135.

26. S. Mathew, A. Yella, P. Gao, R. Humphry-Baker, B. F. Curchod, N. Ashari-Astani, I. Tavernelli, U. Rothlisberger, M. K. Nazeeruddin and M. Grätzel, *Nat. Chem.*, 2014, **6**, 242-247.

27. L.-L. Li and E. W.-G. Diau, *Chem. Soc. Rev.*, 2013, **42**, 291-304.

28. C. V. Kumar, L. Cabau, E. N. Koukaras, G. D. Sharma and E. Palomares, *Nanoscale*, 2015, **7**, 179-189.

29. J. D. Zimmerman, V. V. Diev, K. Hanson, R. R. Lunt, E. K. Yu, M. E. Thompson and S. R. Forrest, *Adv. Mater.*, 2010, **22**, 2780-2783.

30. H.-F. Xiang, S.-C. Yu, C.-M. Che and P. Lai, *Appl. Phys. Lett.*, 2003, **83**, 1518-1520.

31. A. Endo, M. Ogasawara, A. Takahashi, D. Yokoyama, Y. Kato and C. Adachi, *Adv. Mater.*, 2009, **21**, 4802-4806.

32. K. R. Graham, Y. Yang, J. R. Sommer, A. H. Shelton, K. S. Schanze, J. Xue and J. R. Reynolds, *Chem. Mater.*, 2011, **23**, 5305-5312.

33. P. Neuhaus, A. Cnossen, J. Q. Gong, L. M. Herz and H. L. Anderson, *Angewandte Chemie-International Edition*, 2015, **54**, 7344-7348.

34. S. I. Allec, N. V. Ilawe and B. M. Wong, *Journal of Physical Chemistry Letters*, 2016, **7**, 2362-2367.

35. T. Hasobe, S. Fukuzumi and P. V. Kamat, *J. Phys. Chem. B*, 2006, **110**, 25477-25484.

36. J. K. Sprafke, S. D. Stranks, J. H. Warner, R. J. Nicholas and H. L. Anderson, *Angew. Chem. Int. Ed.*, 2011, **50**, 2313-2316.

37. C. Ehli, G. A. Rahman, N. Jux, D. Balbinot, D. M. Guldi, F. Paolucci, M. Marcaccio, D. Paolucci, M. Melle-Franco and F. Zerbetto, *J. Am. Chem. Soc.*, 2006, **128**, 11222-11231.

38. B. Ballesteros, G. de la Torre, C. Ehli, G. Aminur Rahman, F. Agullo-Rueda, D. M. Guldi and T. Torres, *J. Am. Chem. Soc.*, 2007, **129**, 5061-5068.

39. A. Dalui, A. Chakraborty, U. Thupakula, A. H. Khan, S. Sengupta, B. Satpati, D. Sarma, I. Dasgupta and S. Acharya, *J. Phys. Chem. C*, 2016, **120**, 10118-10128.

40. Z. Li, Y. Xiao, Y. Gong, Z. Wang, Y. Kang, S. Zu, P. M. Ajayan, P. Nordlander and Z. Fang, *ACS Nano*, 2015, **9**, 10158-10164.

41. A. El-Sayed, P. Borghetti, E. Goiri, C. Rogero, L. Floreano, G. Lovat, D. J. Mowbray, J. L. Cabellos, Y. Wakayama and A. Rubio, *ACS Nano*, 2013, **7**, 6914-6920.

42. D. H. Kim, H.-J. Shin, H. S. Lee, J. Lee, B.-L. Lee, W. H. Lee, J.-H. Lee, K. Cho, W.-J. Kim and S. Y. Lee, *ACS Nano*, 2011, **6**, 662-670.

43. J. J. Jasieniak, B. B. Hsu, C. J. Takacs, G. C. Welch, G. C. Bazan, D. Moses and A. J. Heeger, *ACS Nano*, 2012, **6**, 8735-8745.

44. A. Hagen, M. Steiner, M. B. Raschke, C. Lienau, T. Hertel, H. H. Qian, A. J. Meixner and A. Hartschuh, *Phys. Rev. Lett.*, 2005, **95**.

45. J. Lefebvre, D. G. Austing, J. Bond and P. Finnie, *Nano Lett.*, 2006, **6**, 1603-1608.

46. L. Cognet, D. A. Tsyboulski, J.-D. R. Rocha, C. D. Doyle, J. M. Tour and R. B. Weisman, *Science*, 2007, **316**, 1465-1468.

47. O. e. Kozák, M. r. Sudolská, G. Pramanik, P. Cígler, M. Otyepka and R. Zbořil, *Chem. Mater.*, 2016, **28**, 4085-4128.

48. B. F. Habenicht and O. V. Prezhdo, *Phys. Rev. Lett.*, 2008, **100**.

49. B. F. Habenicht and O. V. Prezhdo, *J. Am. Chem. Soc.*, 2012, **134**, 15648-15651.

50. S. Pal, D. J. Trivedi, A. V. Akimov, B. l. Aradi, T. Frauenheim and O. V. Prezhdo, *J. Chem. Theory Comput.*, 2016, **12**, 1436-1448.

51. P. V. Parandekar and J. C. Tully, *J. Chem. Phys.*, 2005, **122**, 094102.

52. J. C. Tully, *J. Chem. Phys.*, 1990, **93**, 1061-1071.

53. H. M. Jaeger, S. Fischer and O. V. Prezhdo, *J. Chem. Phys.*, 2012, **137**, 22A545.

54. C. F. Craig, W. R. Duncan and O. V. Prezhdo, *Phys. Rev. Lett.*, 2005, **95**.

55. S. A. Fischer, B. F. Habenicht, A. B. Madrid, W. R. Duncan and O. V. Prezhdo, *J. Chem. Phys.*, 2011, **134**.

56. A. V. Akimov and O. V. Prezhdo, *J. Chem. Theory Comput.*, 2013, **9**, 4959-4972.

57. A. V. Akimov and O. V. Prezhdo, *J. Chem. Theory Comput.*, 2014, **10**, 789-804.

58. B. F. Habenicht, C. F. Craig and O. V. Prezhdo, *Phys. Rev. Lett.*, 2006, **96**, 187401.

59. S. V. Kilina, A. J. Neukirch, B. F. Habenicht, D. S. Kilin and O. V. Prezhdo, *Phys. Rev. Lett.*, 2013, **110**, 180404.

60. K. Hyeon-Deuk and O. V. Prezhdo, *ACS Nano*, 2012, **6**, 1239-1250.

61. S. A. Fischer, W. R. Duncan and O. V. Prezhdo, *J. Am. Chem. Soc.*, 2009, **131**, 15483-15491.

62. V. V. Chaban, V. V. Prezhdo and O. V. Prezhdo, *J. Phys. Chem. Lett.*, 2013, **4**, 1-6.

63. L. Q. Li, R. Long, T. Bertolini and O. V. Prezhdo, *Nano Lett.*, 2017, **17**, 7962-7967.

64. S. Pal, D. Casanova and O. V. Prezhdo, *Nano Lett.*, 2018, **18**, 58-63.

65. Z. S. Zhang, R. Long, M. V. Tokina and O. V. Prezhdo, *J. Am. Chem. Soc.*, 2017, **139**, 17327-17333.

66. X. Zhou, J. Jankowska, L. Q. Li, A. Giri, P. E. Hopkins and O. V. Prezhdo, *ACS Appl. Mater. Interfaces*, 2017, **9**, 43343-43351.

67. A. V. Akimov, J. T. Muckerman and O. V. Prezhdo, *J. Am. Chem. Soc.*, 2013, **135**, 8682-8691.

68. T. Krüger, M. Elstner, P. Schiffels and T. Frauenheim, *J. Chem. Phys.*, 2005, **122**, 114110.

69. G. Seifert, *J. Phys. Chem. A*, 2007, **111**, 5609-5613.

70. B. Aradi, B. Hourahine and T. Frauenheim, *J. Phys. Chem. A*, 2007, **111**, 5678-5684.

71. M. Elstner, *J. Phys. Chem. A*, 2007, **111**, 5614-5621.

72. D. Porezag, T. Frauenheim, T. Köhler, G. Seifert and R. Kaschner, *Phys. Rev. B*, 1995, **51**, 12947.

73. M. Elstner, D. Porezag, G. Jungnickel, J. Elsner, M. Haugk, T. Frauenheim, S. Suhai and G. Seifert, *Phys. Rev. B*, 1998, **58**, 7260.

74. T. A. Niehaus, S. Suhai, F. Della Sala, P. Lugli, M. Elstner, G. Seifert and T. Frauenheim, *Phys. Rev. B*, 2001, **63**, 085108.

75. K. Drukker, *J. Comput. Phys.*, 1999, **153**, 225-272.

76. M. Barbatti, *Wiley Interdiscip. Rev. Comput. Mol. Sci.*, 2011, **1**, 620-633.

77. E. R. Bittner and P. J. Rossky, *J. Chem. Phys.*, 1995, **103**, 8130-8143.

78. O. V. Prezhdo, *J. Chem. Phys.*, 1999, **111**, 8366-8377.

79. S. Mukamel, *Principles of nonlinear optical spectroscopy*, Oxford University Press on Demand, **1999**.

80. T. Frauenheim, G. Seifert, M. Elstner, T. Niehaus, C. Köhler, M. Amkreutz, M. Sternberg, Z. Hajnal, A. Di Carlo and S. Suhai, *J. Phys. Condens. Matter*, 2002, **14**, 3015.

81. R. Sarkar, S. Sarkar, A. Pramanik, P. Sarkar and S. Pal, *RSC Adv.*, 2016, **6**, 86494-86501.

82. S. Sarkar, S. Pal, P. Sarkar, A. Rosa and T. Frauenheim, *J. Chem. Theory Comput.*, 2011, **7**, 2262-2276.

83. L. Zhechkov, T. Heine, S. Patchkovskii, G. Seifert and H. A. Duarte, *Journal of Chemical Theory and Computation*, 2005, **1**, 841-847.

84. L. Verlet, *Phys. Rev.* , 1967, **159**, 98.

85. F. A. Walker, *J. Am. Chem. Soc.*, 1973, **95**, 1150-1153.

86. E. Rabani, R. Baer and D. Neuhauser, *Phys. Rev. B*, 2015, **91**, 235302.

87. C. Attaccalite, M. Grüning and A. Marini, *Phys. Rev. B*, 2011, **84**, 245110.

88. H. Zhao and S. Mazumdar, *Phys. Rev. Lett.*, 2004, **93**, 157402.

89. J. Maultzsch, R. Pomraenke, S. Reich, E. Chang, D. Prezzi, A. Ruini, E. Molinari, M. Strano, C. Thomsen and C. Lienau, *Phys. Rev. B*, 2005, **72**, 241402.

90. Z. Wang, H. Pedrosa, T. Krauss and L. Rothberg, *Phys. Rev. Lett.*, 2006, **96**, 047403.

91. X. Liu, C. Huang and M. Li, *J. Phys. Chem. C*, 2016, **120**, 27148-27158.

92. H.-J. Son, S. Jin, S. Patwardhan, S. J. Wezenberg, N. C. Jeong, M. So, C. E. Wilmer, A. A. Sarjeant, G. C. Schatz and R. Q. Snurr, *J. Am. Chem. Soc.*, 2013, **135**, 862-869.

93. S. D. Stranks, J. K. Sprafke, H. L. Anderson and R. J. Nicholas, *ACS Nano*, 2011, **5**, 2307-2315.

94. T. S. Rush, P. M. Kozlowski, C. A. Piffat, R. Kumble, M. Z. Zgierski and T. G. Spiro, *J. Phys. Chem. B*, 2000, **104**, 5020-5034.

95. S. Malola, H. Häkkinen and P. Koskinen, *Phys. Rev. B*, 2008, **77**, 155412.

96. J. E. Donehue, O. P. Varnavski, R. Cemborski, M. Iyoda and T. Goodson, *J. Am. Chem. Soc.*, 2011, **133**, 4819-4828.

97. B. F. Habenicht, H. Kamisaka, K. Yamashita and O. V. Prezhdo, *Nano Lett.*, 2007, **7**, 3260-3265.

98. H. Yoo, J. Yang, Y. Nakamura, N. Aratani, A. Osuka and D. Kim, *J. Am. Chem. Soc.*, 2009, **131**, 1488-1494.

99. J. S. Hsiao, B. P. Krueger, R. W. Wagner, T. E. Johnson, J. K. Delaney, D. C. Mauzerall, G. R. Fleming, J. S. Lindsey, D. F. Bocian and R. J. Donohoe, *J. Am. Chem. Soc.*, 1996, **118**, 11181-11193.

Table of Contents graphic

Defect-free porphyrin/CNT hybrids can maintain long-lived charge separation; porphyrin and CNT can be used to harvest light at different wavelengths.